Laser texturing of Li-ion battery electrode current collectors for improved active layer interface adhesion

Contents lists available at SciVerse ScienceDirect

CIRP Annals Manufacturing Technology

Journal homepage: www.elsevier.com/locate/cirp

Laser texturing of Li-ion battery electrode current collectors for improved active layer interface adhesion

Luca Romoli (2), Adrian H.A. Lutey, Gianmarco Lazzini

Department of Engineering and Architecture, University of Parma, 43124 Parma, Italy

Nanosecond laser processing (NLP) is performed on aluminium and copper Li-ion battery (LIB) current collectors to improve the interface adhesion with active materials. The developed area ratio, S_{dr}, void volume, V_v, and maximum crater depth, h, are introduced to quantify the effectiveness and feasibility of NLP over a range of process parameters. By limiting the crater depth to half the foil thickness, increases in surface area of 20% and 13% are achieved on aluminium and copper foils of thickness 30 µm and 10 µm with a fluence of 24.8 J/cm² and 49.5 J/cm², respectively. The adhesion ratio of intact active material following peel-off tests on complete electrodes with textured current collectors is approximately 30% higher than with untreated current collectors.

Laser; Texture; Li-ion Battery

1. Introduction

Lithium-ion batteries (LIBs) are ubiquitous in everyday life as electrochemical energy storage systems and are poised to play a fundamental role in transport and power transmission systems over the next decade [1]. The compelling challenge is currently the production of batteries with high volumetric energy density, high volumetric power density, long service life and low life-cycling impact [2].

The basic components of a LIB are the anode, cathode, separator and electrolyte. The anode and cathode have the role of conductors, the separator inhibits contact between the electrodes to avoid short-circuits and the electrolyte is the medium through which ions and electrons propagate [3]. In commercial LIBs, the anode is made up of a copper foil coated with an active material that typically comprises graphite mixed with an electronic conductivity enhancer such as carbon black [4,5]. The cathode is instead made up of an aluminium foil coated with an active material that depends on the cell chemistry, such as $LiCO_2$ (LCO), $LiNiMnCoO_2$ (NMC), $LiNiCoAlO_2$ (NCA) or $LiFePO_4$ (LFP), mixed with carbon black [4]. Both the anode and cathode are produced by depositing a slurry of active material in powder form mixed with a binder and solvent onto the metallic current collector. A drying procedure is then required to remove the solvent from the slurry.

To obtain high energy density and long service life, sufficient adhesion strength between the active material and metallic current collector must be ensured. Further to minimizing electrical resistance, this aspect is essential for avoiding delamination from rolling during assembly or volumetric changes during charging and discharging [6]. The latter has substantial implications for the uptake of higher density active materials such as silicon anodes [7], as well as water-based binders with lower environmental footprint than current solutions.

To improve interface adhesion, it is possible to increase the binder concentration; however, the lower proportion of active material and higher viscosity of the resulting slurry reduce cell performance and make implementation difficult in large-scale production due to greater energy requirements for the drying phase [8]. For this reason, alongside research aimed at identifying novel and high-performance binders [9], generation of roughness on the metallic current collector surface is an effective approach for increasing the available contact area and therefore adhesion between the active material and current collector. This provides potential to expand the range of cell chemistries to include those that undergo larger volumetric changes during cycling. Among available technologies, laser processing offers several advantages in terms of precision and industrial implementation [6,10].

Ultrashort laser processing (ULP) of aluminium and copper current collectors has been explored as an approach for generating sub-micrometric protrusions [6]. This technology, however, exhibits important limitations in terms of cost and penetration of high-viscosity slurries [8] into sub-micrometric laser-induced surface structures. Nanosecond laser processing (NLP) is a low-cost alternative for large-scale production of textured current collectors. This approach has been proven to be effective on 150 µm thick copper foils [11]. Ablation phenomena taking place during NLP increase the available contact area at the interface by increasing surface roughness. Careful attention must be paid to the integrity of current collectors, especially when dealing with metallic foil thicknesses in the order of 10-40 µm adopted in modern high energy density LIBs. Considering the flexibility of such thin electrodes, which undergo rolling procedures during cell assembly, interface shear resistance is of utmost importance to avoid failure [12].

Based on these considerations, this work focuses on NLP of aluminium and copper current collectors as an approach for improving interface adhesion between LIB current collectors and active material layers. Improved interface adhesion is expected to enhance the service life of existing LIB chemistries and provide new possibilities for the uptake of higher energy density active materials. The main idea is to provide better penetration of the slurry into the morphology of the textured current collector and enhance interlocking phenomena at the interface once the electrode has dried. The influence of surface topography on adhesion phenomena requires an analytical description in terms of available contact area, maximum crater depth and ablated volume. The final objective of this work is to compare electrodes fabricated with textured and untextured current collectors and to

demonstrate that improvements in adhesion between active material layers and laser-textured current collectors are obtainable without adversely affecting the charge capacity of LIBs.

2. Materials and methods

2.1. Laser texturing

NLP was carried out on aluminium foil of thickness 30 µm and copper foil of thickness 10 µm, representing typical cathode and anode current collectors with thickness chosen to maximise volumetric energy density while ensuring sufficient electrical conductivity and mechanical strength. To avoid the formation of creases during texturing, the foils were held flat on a 3 mm thick steel substrate by wetting the interface with distilled water prior to laying out the foils. An Ytterbium-doped fibre laser with a wavelength of 1064 nm, pulse duration of 104 ns, beam quality (M^2 factor) of 1.8 and repetition rate of 20 kHz was used for experiments, with all treatments performed in air. A galvanometric scanning head with a 160 mm focal length f-theta lens was used to scan the focused beam over an area of 70 mm × 25 mm on the sample surface in a raster trajectory. The focused Gaussian spot diameter was 60 µm and the Rayleigh length 1.5 mm. The scanning speed (1.2 m/s) and hatch spacing (60 µm) were chosen to achieve longitudinal and lateral pulse spacings equal to the focused laser spot diameter. This scanning strategy has been shown to provide the largest increase in surface area for a given ablation depth [13]. Throughput was 72 mm^2/s with the employed configuration. Variable process parameters employed for experiments are summarised in Table 1. Laser power and therefore pulse energy were limited to ranges where ablation craters could be observed but large-scale melting or complete penetration of the films did not take place.

Table 1. Process parameters employed for NLP of aluminium and copper.

Current collector	Al	Cu
Laser power (W)	4-11	10-17
Pulse energy (µJ)	200-550	500-850
Peak pulse fluence (J/cm^2)	14.1-38.9	35.4-60.1

The obtained surfaces comprised a series of adjacent craters with raised lateral ridges and submicrometric particles due to solidification of material ejected from the ablated area. Features therefore ranged from less than 1 µm to tens of µm in size. Considering the thickness of the deposited slurry, typically in the order of 40-100 µm, and the consistency of the dried active layer, the crater shape was expected to play a fundamental role in determining the contact area between the slurry and current collector, and therefore the interface adhesion upon drying.

2.2. Surface analysis

The surface topography of the metallic foils obtained with NLP was analysed with a Taylor Hobson CCI-MP Coherence Scanning Interferometer (CSI) equipped with a 50× objective. The horizontal and vertical resolution of the instrument were <0.6 µm and <1 nm, respectively. Filtering of acquired data included levelling of the surface profile based on a least-squares plane and interpolating a limited number of unmeasured points (maximum 1.5% of the total) due to local inclination of the surface in proximity of the ablation craters. Specific areal roughness parameters were calculated in line with ISO 25178 to quantitatively assess outcomes in terms of surface area and void volume. The developed area ratio, $S_{dr} = (A - A_{proj})/A_{proj}$, was used to quantify the increase in surface area, A, with respect to the projected surface area on the mean plane, A_{proj}, corresponding to a perfectly flat surface. Due to the low roughness of the metallic foils (S_a < 0.1 µm), A_{proj} was considered a reasonable approximation of the surface area of the untreated substrate. Larger values of S_{dr} therefore indicated that NLP was able to significantly increase the surface area compared to the untreated foil, with positive implications in terms of adhesion strength [14].

For a given increase in surface area, the feasibility and efficiency of surface texturing of thin foils depends strongly on the maximum crater depth and ablated volume. The maximum crater depth, h, was defined as the difference between the mean height of the untreated surface and the maximum depth of ablation craters, averaged over nine individual craters. As a conservative limit, the maximum value of h was considered as half the thickness of the metal foil to avoid perforation. The ablated volume was instead quantified in terms of the void volume, V_v [15], defined as the volume of space bounded by the surface and a horizontal plane corresponding to a given material ratio (mr), divided by the projected surface area, A_{proj}. With an appropriate choice of mr, V_v can be interpreted as the ablated volume per unit area of the original flat surface in $\mu m^3/\mu m^2$. A value of mr = 0.1 was chosen for all surfaces to achieve approximate correspondence between the original surface and the horizontal plane used for calculation of V_v, thus excluding raised ridges and re-solidified material above the original flat surface. This value was determined using surface profiles obtained with the optical profiler at the edges of the textured regions, where the reference plane height was compared with the original surface height. A schematic of the aforementioned parameters for a single ablation crater is presented in Figure 1, together with the corresponding Abbott curve.

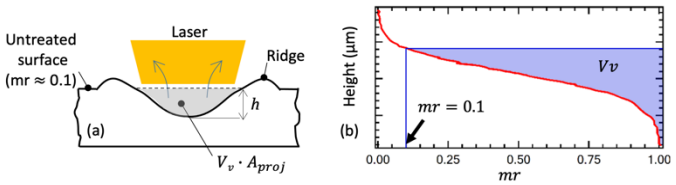

Figure 1. (a) Schematic of a single ablation crater with maximum crater depth h and total ablated volume $V_v \cdot A_{proj}$; (b) Corresponding Abbott curve with $mr = 0.1$ and void volume V_v.

2.3. Adhesion tests

The effectiveness of laser texturing in terms of improved interface adhesion was assessed by depositing slurries on textured and untextured current collectors and performing peel-off tests on the dried electrodes. Based on the results of surface morphology analysis with the parameter combinations in Table 1, laser texturing was performed to achieve the largest increase in surface area (S_{dr}) without exceeding a maximum crater depth (h) of 15 µm for aluminium and 5 µm for copper, corresponding to half the foil thickness. A slurry comprising 70% LFP, 20% carbon black and 10% carboxymethylcellulose (CMC) was prepared for the cathode (aluminium) and a slurry comprising 90% graphite and 10% CMC was prepared for the anode (copper). Both were suspended in water and deposited onto cleaned textured and untextured current collectors with a Sheen 1133N automatic film applicator to achieve a uniform dried layer thickness of 40 µm ± 10 µm. The electrodes were held at 70°C for one hour and a further 24 hours at room temperature prior to peel-off tests. A 10 mm × 10 mm area of each electrode was laser cut, mounted vertically in resin, lapped and polished to allow Scanning Electron Microscope (SEM) analysis of the section.

Peel-off tests were employed to compare adhesion of the deposited active material on textured and untextured current collectors. Adhesive tape was placed over 70 mm × 25 mm strips of the complete electrodes, with constant pressure applied over the tested area with a roller tool. The tape was then peeled off at an angle of 180° under a controlled load of 1.5 N, as represented schematically in Fig. 2. Damage to electrodes with textured and untextured current collectors was then compared by measuring the percentage area of intact active material remaining on the current collector after the peel-off test. This percentage, obtained via image processing of photographs in software ImageJ, was defined as the adhesion ratio (*RA*). A value of 100% indicated a completely intact electrode, while a value of 0% indicated that all active material had been removed during the peel-off test.

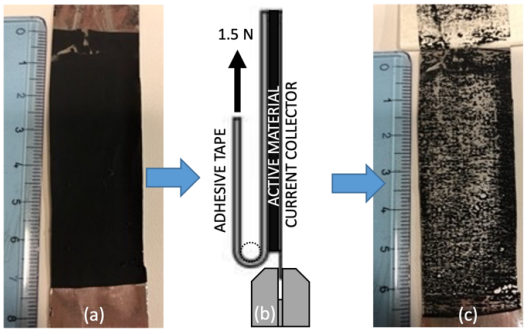

Figure 2. (a) Image of complete electrode with active material layer on aluminium foil. (b) Schematic of 180° peel-off test according to ASTM D 3167. (c) Image of electrode after the test, used to determine *RA*.

3. Results and discussion

Figure 3 presents acquired surface profiles of the aluminium and copper foils following NLP at F = 24.8 J/cm² and F = 49.5 J/cm², respectively. The surfaces are characterised by craters arranged in a square grid, with each crater surrounded by an irregular ridge comprising re-solidified material forced outwards from the crater axis during rapid heating and pressure rise following nanosecond pulsed laser exposure.

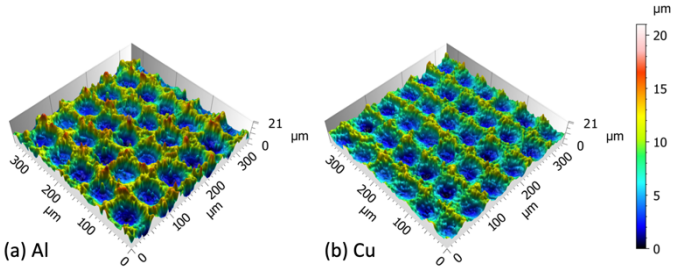

Figure 3. Topographic maps of current collectors following NLP: (a) aluminium foil textured with F = 24.8 J/cm²; (b) copper foil textured with F = 49.5 J/cm².

Figure 4 presents the developed area ratio, S_{dr}, maximum crater depth, h, and void volume, V_v, of the textured aluminium and copper foils over the tested parameter range. The parameter S_{dr} increases quickly at low fluence for both copper and aluminium as the crater depth and width increase rapidly above the ablation threshold. A maximum value of S_{dr} = 0.20 is achieved on aluminium for F = 24.8 J/cm², implying a 20% increase in surface area compared to the untreated foil. At high fluence, S_{dr} decreases for the same material due to amalgamation of adjacent ablation craters. F = 24.8 J/cm² was therefore chosen for subsequent adhesion tests performed on aluminium as an increase in the surface area was expected to improve adhesion [14]. The value of S_{dr} instead continued to increase for copper at high fluence, albeit more slowly, as amalgamation of adjacent ablation craters did not take place due to the higher ablation threshold of copper at a wavelength of 1064 nm. The selected value of fluence for subsequent adhesion tests was therefore F = 49.5 J/cm², chosen to obtain a maximum value of S_{dr} = 0.13 without the crater depth exceeding half the copper foil thickness (5 μm).

The maximum crater depth, h, increases logarithmically with F for both aluminium and copper. While h remains below the foil thickness in all cases, 30 μm for aluminium and 10 μm for copper, the parameter exceeds 5 μm for fluence levels above 50 J/cm² on copper. The void volume, V_v, also increases logarithmically but with a lower gradient at high fluence compared to h. Changes in measured values of V_v were within the range of experimental error for aluminium at fluence levels above 25 J/cm². This effect is due to a rapid initial increase in both crater depth and diameter at low fluence followed by more limited increases in crater depth and virtually no increases in diameter beyond the focused spot diameter at high fluence. Over the tested parameter range, maximum values of void volume were V_v ~ 5 μm³/μm² for aluminium and V_v ~ 4 μm³/μm² for copper, implying that the average material removal depth under these conditions was 5 μm and 4 μm, respectively.

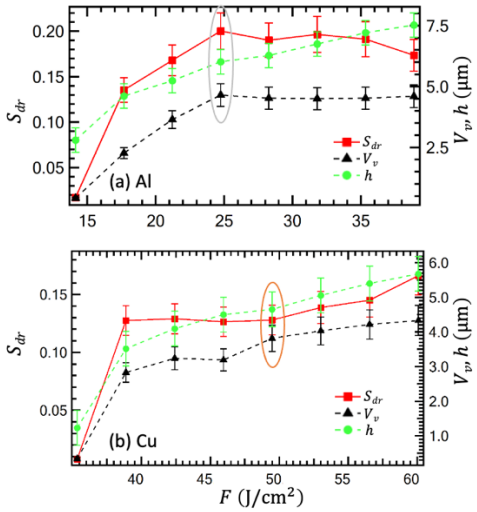

Figure 4. (a) S_{dr}, V_v and h versus fluence, F, for laser-textured surfaces on (a) aluminium and (b) copper foils. Parameters chosen for subsequent electrode assembly are highlighted for each electrode.

The ratio S_{dr}/V_v provides useful insight into the efficiency with which increases in surface area can be achieved for a given ablated volume. This value was 0.04 μm⁻¹ for aluminium at F = 24.8 J/cm² and 0.03 μm⁻¹ for copper at F = 49.5 J/cm², implying that the percentage increase in surface area achieved per μm of average ablation depth was 4% and 3%, respectively, under these conditions. These values provide physical limits for the increase in surface area that can be achieved with a given foil thickness and may justify using thicker current collectors should larger increases in surface area be required. Furthermore, the ratio S_{dr}/V_v is directly related to the aspect ratio of surface features and is therefore expected to increase as the feature size decreases [13]. This outcome favours the use of the smallest possible laser spot size for NLP should increases in adhesion performance justify the adoption of more precise optical collimation or higher beam quality.

Figure 5 presents SEM images of electrode sections obtained with laser-textured current collectors produced with the aforementioned parameters. Pore-free active material layers (in black) can be observed on both electrodes, with complete penetration of the active material into laser-generated surface features on the current collectors (in grey). Considering the

presence of raised ridges around the ablation craters (Fig. 3), the depths of the observed craters in SEM images are in line with measured values obtained with the optical profiler (Fig. 4). The total thicknesses of the complete cathode and anode with textured current collectors are approximately 65 µm and 55 µm, respectively. Considering the initial thickness of the aluminium and copper foils, 30 µm and 10 µm, respectively, the thickness of the deposited layer was approximately 35 µm on the cathode and 45 µm on the anode.

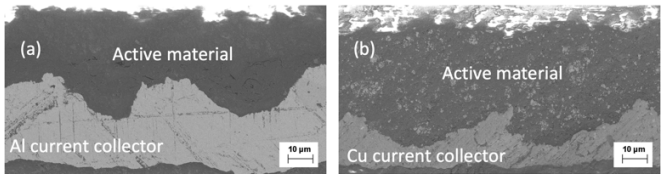

Figure 5. SEM images of electrode sections for complete: (a) cathode and (b) anode with textured current collectors.

Complete penetration of the slurry into the surface morphology during deposition on both electrodes, as observed in SEM analysis, led to improved adhesion between the active material and current collector on both electrodes. Values of adhesion ratio, *RA*, obtained during peel-off tests are provided in Fig. 6. The laser treatment resulted in an increase in *RA* of about 30% for both textured aluminium and copper current collectors compared to untreated samples. *RA* data dispersion over five tests performed on electrodes with untextured current collectors was approximately 10%. This was related to the higher uncertainty of cracking phenomena leading to delamination from the smooth surface of the metal foil (S_a < 0.1 µm) and removal of relatively large flakes. Conversely, craters on the laser-textured foils inhibited complete detachment of the layer and thus resulted in better interlocking phenomena at the interface and lower dispersion of *RA* data. In particular, the most evident effect was found on the Cu substrates, where negligible coating removal was observed on the textured electrode. Differences in *RA* between the anode and cathode are likely due to the mechanical properties of the materials involved, with graphite and CMC deposited on copper exhibiting higher intrinsic adhesion than LFP, carbon black and CMC deposited on aluminium. The employed peel-off test nonetheless achieved sufficient sensitivity to demonstrate a clear improvement in adhesion on the laser-textured electrodes.

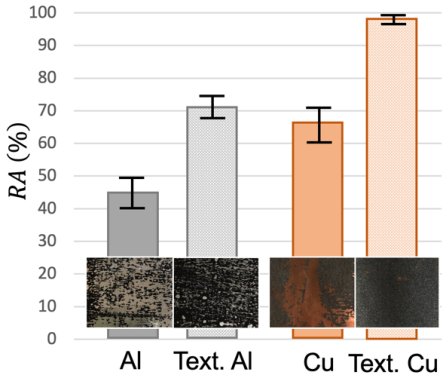

Figure 6. Measured values of *RA* and images of electrodes produced with textured and untextured current collectors following peel-off tests.

4. Conclusion

The outcomes obtained within this study imply that NLP is an effective approach for increasing the interface adhesion between LIB current collectors and active materials, with the *RA* following peel-off tests some 30% higher for electrodes with textured current collectors compared to unmodified electrodes. Evaluation of the developed area ratio, S_{dr}, maximum crater depth, h, and void volume, V_v, on textured surfaces provides quantitative standardised benchmarks for the comparison of surface profiles obtained with different laser systems and process parameters. By limiting the crater depth to no more than half the foil thickness, maximum increases in surface area of 20% and 13% were obtained on aluminium and copper foils, respectively, with a 60 µm laser spot size. Use of a smaller spot size is likely to improve this outcome by increasing the aspect ratio of ablation craters.

Preliminary tests performed on coin cells with the same laser-textured LFP cathodes presented in this study have exhibited comparable performance to cells produced without textured current collectors, suggesting that laser texturing does not adversely affect the charge capacity. The true value of laser texturing, however, is likely to become evident when applied to electrodes with higher energy density active materials such as silicon, where volumetric changes during charge and discharge cycling currently cause rapid capacity degradation, which is in part due to delamination. Investigation into laser texturing as an approach for improving the feasibility of new active materials therefore holds much potential for future research.

Acknowledgements

The authors are grateful to Prof. Silvia Bodoardo and Dr. Daniele Versaci (Electrochemistry Group – Politecnico di Torino, Italy) for electrode assembly and preliminary tests performed on coin cells.

References

[1] Grey CP, Hall DS (2020) Prospects for lithium-ion batteries and beyond-a 2030 vision. *Nat Commun* 11(1):6279.
[2] Yuan C, Cao H, Shen K, Deng Y, Zeng D, Dong Y, Hauschild M (2021) Water-based manufacturing of lithium ion battery for life cycle impact mitigation. *CIRP Ann* 70(1): 25-28.
[3] Chen Y, Kang Y, Zhao Y, Wang L, Liu J, Li Y, Liang Z, He X, Li X, Tavajohi N, Li B (2021). A review of lithium-ion battery safety concerns: The issues, strategies, and testing standards. *J Energy Chem* 59: 83-99.
[4] Zhu J, Li W, Wierzbicki T, Xia Y, Harding J (2019) Deformation and failure of lithium-ion batteries treated as a discrete layered structure. *Int J Plasticity* 121: 293-311.
[5] Nirmale TC, Kale BB, Varma AJ (2017) A review on cellulose and lignin based binders and electrodes: Small steps towards a sustainable lithium ion battery. *Int J Biol Macromol* 103: 1032-1043.
[6] Wang Y, Zhao Z, Zhong J, Wang T, Wang L, Xu H, Cao J, Li J, Zhang G, Fei H, Zhu J (2021) Hierarchically micro/nanostructured current collectors induced by ultrafast femtosecond laser strategy for high-performance lithium-ion batteries. *Energy & Environmental Materials* 0, 1-8.
[7] Pfleging W (2018) A review of laser electrode processing for development and manufacturing of lithium-ion batteries. *Nanophotonics* 7(3): 549-573.
[8] Jeschull F, Brandell D, Wohlfahrt-Mehrens M, Memm M (2017) Water-soluble binders for lithium-ion battery graphite electrodes: slurry rheology, coating adhesion, and electrochemical performance. *Energy Technol* 5(11): 2108-2118.
[9] Guo R, Zhang S, Ying H, Yang W, Wang J, Han WQ (2019) New, effective, and low-cost dual-functional binder for porous silicon anodes in lithium-ion batteries. *ACS Appl Mater Inter*, 11(15): 14051-14058.
[10] Romoli L, Moroni F, Khan MMA (2017) A study on the influence of surface laser texturing on the adhesive strength of bonded joints in aluminium alloys. *CIRP Ann* 66(1): 237-240.
[11] Tang X, Liu W, Ye B, Tang Y (2013) Preparation of current collector with blind holes and enhanced cycle performance of silicon-based anode. *T Nonferr Metal Soc* 23: 1723-1727.
[12] Li X, Zeng T, Qin H, Huo R, Liu Y, Wei D, Ding X (2021) Investigation of inhomogeneous degradation in large-format lithium-ion batteries. *Journal of Energy Storage* 42: 103113.
[13] Lutey A, Romoli L (2019) Surface topography following pulsed laser texturing: Implications for adhesion and wettability. *Surf Topogr: Metrol Prop* 7(4): 045023.
[14] Kromer R, Costil S, Cormier J, Courapied D, Berthe L, Peyre P, Boustie M (2015). Laser surface patterning to enhance adhesion of plasma sprayed coatings. *Surf Coat Tech* 278: 171-182.
[15] Lou S, Zhu Z, Zeng W, Majewski C, Scott PJ, Jiang X (2021). Material ratio curve of 3D surface topography of additively manufactured parts: an attempt to characterise open surface pores. *Surf Topogr: Metrol Prop* 9(1): 015029.